Available online at www.sciencedirect.com
SCIENCE DIRECT®
Journal of Sound and Vibration 288 (2005) 523–549
JOURNAL OF SOUND AND VIBRATION
www.elsevier.com/locate/jsvi

Assessment of uncertainty on structural dynamic responses with the short transformation method

S. Donders[a,*], D. Vandepitte[b], J. Van de Peer[c], W. Desmet[b]

[a]*LMS International, CAE Division, Interleuvenlaan 68, B-3001 Leuven, Belgium*
[b]*Department of Mechanical Engineering, Katholieke Universiteit Leuven (K.U. Leuven), Division PMA, Celestijnenlaan 300B, B-3001 Leuven, Belgium*
[c]*Noesis Solutions, Interleuvenlaan 68, B-3001 Leuven, Belgium*

Accepted 5 July 2005
Available online 1 September 2005

Abstract

The predictive capability of finite element models is limited by their deterministic nature: typically, not all model parameters are exactly known, while even small deviations may have significant effects on the predicted response. Parameter uncertainty should therefore be taken into account, e.g. with fuzzy arithmetic. The absence of fuzzy solvers led to interval arithmetic as a numerical alternative. The Transformation Method (TM), presented by M. Hanss, replaces interval arithmetic with a set of deterministic computations: for each interval, all parameter extrema are combined in every possible way. In a Design of Experiments terminology, the TM is a so-called Full Factorial design.

The TM is applicable if the output is monotonic in the inputs. Unlike interval arithmetic, it does not overestimate the response uncertainty, as only parameter combinations are evaluated that actually occur. In this paper, the TM has been applied to visualise uncertain frequency response functions (FRFs), obtained with modal superposition. This yields accurate results when validated against Monte Carlo data, but the computation time is rather high. The Short Transformation Method (STM) is proposed as an attractive alternative to the original TM. A full set of deterministic computations, combining all interval extrema, is only performed at the lowest interval. For higher levels, a smaller set is evaluated. This allows

*Corresponding author. Fax: +32 16 384 505.
E-mail addresses: stijn.donders@lms.be (S. Donders), dirk.vandepitte@mech.kuleuven.ac.be (D. Vandepitte), joost.vandepeer@noesis.be (J. Van de Peer), wim.desmet@mech.kuleuven.ac.be (W. Desmet).

0022-460X/$ - see front matter
doi:10.1016/j.jsv.2005.07.003

reconstructing the fuzzy FRF from a much lower number of deterministic computations, with only a small reduction in the accuracy of FRFs. Both methods are demonstrated on a clamped plate and a car front cradle with uncertain design parameters.

1. Introduction

Nowadays, product design departments in automotive industry are using finite element (FE) models intensively to analyse and solve a variety of engineering problems related to the vehicle noise and vibration performance. These large numerical models are deterministic, i.e. it is implicitly assumed that all parameters are precisely known and that the manufacturing process produces identical structures. This is typically not valid, as two classes of parameter deficiency can be distinguished [1]. *Variability* refers to the variation inherent to the physical system or the environment under consideration, while *uncertainty* is a potential deficiency in any phase or activity of the modelling process that is due to lack of knowledge. Variability typically exists on the level of physical properties (geometric, material characteristics) and manufacturing tolerances, while uncertainty exists on the level of model inaccuracy (e.g. joint models between subsystems) and physical properties in an early design stage, when design decisions must still be taken, so that dimensions and material properties are not yet fixed. Increasing the knowledge may reduce uncertainty, whereas variability is an irreducible scatter on the parameter value. As even small parameter changes may have substantial effects on response predictions, a reliable method to assess the effect of uncertainty and variability is very important [2,3]. Variability is typically modelled with a probability density function (PDF); its effect can be assessed with well-established stochastic procedures. Uncertainty should not be described in a probabilistic manner: there is not enough information available, so that assigning a PDF changes the problem definition in a subjective way. The results may be erroneous, and there is no way to verify this from the obtained results.

A suitable way to take uncertainty into account is with a possibilistic approach, such as *fuzzy arithmetic*, which allows to identify worst-case scenarios without assigning a level of probability to the set of possible outcomes. Two paths can be distinguished regarding the application of fuzzy arithmetic to structural dynamics problems. The first path is to completely replace conventional arithmetic with a generalized fuzzy arithmetic [4,5]. This allows to assemble fuzzy system matrices and perform a fuzzy modal analysis [6]. Such a procedure is; however, limited to rather academic problems, as fuzzy solvers are either slow or non-existing; for example, fuzzy matrix inversion is not (yet) possible. Numerical approximations have therefore been developed; the α-sublevel technique allows to numerically represent a fuzzy number by a set of intervals, so that *interval arithmetic* [7] can be used to estimate an interval representation on the problem's output side. Unfortunately, this procedure often leads to overestimation of the output uncertainty. A fuzzy eigenvalue analysis method based on interval arithmetic, using an optimization procedure to prevent this overestimation, has been presented in Ref. [8].

The second path is based on Design of Experiments (DOE) methodology and conventional arithmetic. A DOE is a set of experiments, designed to provide maximal information using minimal computational effort [9]. The Vertex Method [10] performs a full-factorial DOE on the

input vertex of the fuzzy problem. Each of the n input parameters is either assigned its minimum or its maximum value, and all possible combinations of individual parameter minima or maxima are listed. Each of the 2^n parameter combinations is then successively analysed in a conventional deterministic analysis run, and the fuzzy output is reconstructed from the deterministic results. The Reduced Transformation Method [11] is an extension of the Vertex Method: the fuzzy inputs are subdivided into a number of intervals, and a Full Factorial DOE is performed for each of these intervals. Hanss also presented the General Transformation Method [11] that adds more points to the DOE. This method has not been considered; in the remainder of this paper, the term "Transformation Method" (TM) denotes the reduced form. When compared to completely fuzzy approaches, the DOE-based approaches have the advantage that much less algorithm development is required, as the bulk part of the fuzzy problem is solved with standard deterministic computations.

In this paper, the TM is applied to predict the frequency response function (FRF) of dynamic structures with uncertain input parameters. Existing FE routines can thus be used to solve the bulk part of the structural analysis. The fuzzy FRF is obtained from a set of deterministic FRFs, where each FRF is obtained with a modal superposition of modal contributions within the frequency range of interest [12]. For uncertain parameters with a global effect on the structure, the *eigenfrequency values* are perhaps monotonic in the inputs, while the *amplitude at given frequency* typically does not depend on the inputs in a monotonic way. The *Short Transformation Method* (STM) is introduced in this paper as a computationally attractive alternative to the original TM, for dynamic analysis of structures with uncertain parameters that affect the eigenfrequency values in a (more or less) monotonic way.

2. Fuzzy sets and numbers

In classical set theory, the elements x of a set A either belong to the set entirely, i.e. the membership level is $\mu_A = 1$, or do not belong to the set at all, so that $\mu_A = 0$. This principle is generalized in *fuzzy set* theory: a membership level $\mu_A(x) \in [0, 1]$ is assigned to all elements x, i.e. the elements belong to the set to a certain degree. The *core* of the set is defined as the subset for which $\mu_A = 1$. The *support* is the subset for which $\mu_A > 0$ (also known as the *input vertex*). The α-*cut* is a generalized support: the subset for which $\mu_A \geqslant \alpha$. A *fuzzy number* is a fuzzy set with some specific properties: the set is convex and normal, the membership function is piecewise continuous, and the core consists of a single element [13]. A fuzzy number's membership function can be of arbitrary shape, either derived from (limited) experimental data or expert knowledge of the model parameters. Fig. 1 shows two well-established types: a membership function with a Gaussian and a triangular shape. The triangular shape is widely used for reasons of simplicity: when the exact parameter distribution is not known, it does not make sense to assign a more complex-shaped function.

As mentioned in the introduction, the α-sublevel technique is often used to numerically represent a fuzzy number [4]. The membership range of all fuzzy numbers is subdivided into α-sublevels at membership levels

$$\mu_j = j \cdot \Delta\mu, \quad \text{for } j = 0, 1, \ldots, m, \text{ where } \Delta\mu = 1/m. \tag{1}$$

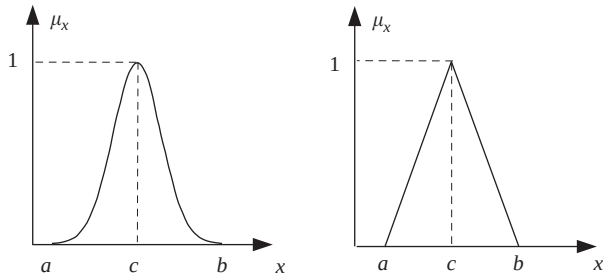

Fig. 1. Fuzzy numbers with Gaussian (left) and triangular (right) membership function $\mu_A(x)$. The core is denoted as c, the support is the interval $[a, b]$.

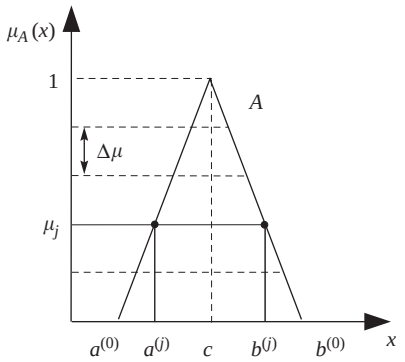

Fig. 2. The α-sublevel technique to numerically represent a fuzzy number with membership function $\mu_A(x)$ as a set of intervals $[a^{(j)}, b^{(j)}]$ at membership levels μ_j.

The intersection of each membership function at the level $\mu_j = \alpha$ yields an interval $[a^{(j)}, b^{(j)}]$ for which the membership value $\mu_j \geqslant \alpha$. The set of $m+1$ intervals (note that the core level $\mu_A = 1$ is included) can then be used to numerically represent the original fuzzy number. Fig. 2 demonstrates this technique for a triangular fuzzy number, subdivided into 4 intermediate intervals, next to core (at $\mu_A = 1$) and support (at $\mu_A = 0$), so that $m = 5$.

3. The Transformation Method

This section gives an outline of the (reduced) TM, as presented in the paper of Hanss [11]. Consider an arithmetic function $f(\cdot)$ that depends on n uncertain parameters $x_1, x_2, \ldots, x_n$, so that the function output $q = f(x_1, x_2, \ldots, x_n)$ is a fuzzy number as well. The n parameters are modelled as fuzzy numbers $\tilde{p}_i,\ i = 1, 2, \ldots, n$ with a membership function $\mu_A(x)$ of arbitrary shape. Using the α-sublevel method (see Section 2), each of the parameters is decomposed into a set P_i of $m+1$ intervals $X_i^{(j)},\ j = 0, 1, \ldots, m$ of the form

$$P_i = \{X_i^{(0)}, X_i^{(1)}, \ldots, X_i^{(m)}\} \tag{2}$$

with

$$X_i^{(j)} = [a_i^{(j)}, b_i^{(j)}], \quad a_i^{(j)} \leqslant b_i^{(j)}, \ i = 1, 2, \ldots, n, \ j = 0, 1, \ldots, m. \tag{3}$$

The intervals are then transformed into arrays $\hat{X}_i^{(j)}$ of the following form:

$$\hat{X}_i^{(j)} = \underbrace{(\alpha_i^{(j)}, \beta_i^{(j)}, \alpha_i^{(j)}, \beta_i^{(j)}, \ldots, \alpha_i^{(j)}, \beta_i^{(j)})}_{2^{i-1} \text{ pairs}} \tag{4}$$

with

$$\alpha_i^{(j)} = \underbrace{(a_i^{(j)}, \ldots, a_i^{(j)})}_{2^{n-i} \text{ elements}}, \quad \beta_i^{(j)} = \underbrace{(b_i^{(j)}, \ldots, b_i^{(j)})}_{2^{n-i} \text{ elements}}, \tag{5}$$

where $a_i^{(j)}$ and $b_i^{(j)}$ denote the lower and upper bound of the interval at the membership level μ_j for the ith uncertain parameter. For each interval level, these arrays combine the interval extrema $a_i^{(j)}$ and $b_i^{(j)}$ in every possible way, in a regularity similar to a Full Factorial DOE. For an example problem with 3 uncertain parameters, the arrays $\hat{X}_i^{(j)}$ in Eq. (4) are given by $\hat{X}_1^{(j)}$, $\hat{X}_2^{(j)}$ and $\hat{X}_3^{(j)}$ in Eq. (6); the 2^3 columns of $\hat{X}_i^{(j)}$ have the regularity of a Full Factorial DOE.

$$\left\{ \begin{matrix} \hat{X}_1^{(j)} \\ \hat{X}_2^{(j)} \\ \hat{X}_3^{(j)} \end{matrix} \right\} = \left\{ \begin{matrix} (a_1^{(j)}, a_1^{(j)}, a_1^{(j)}, a_1^{(j)}, b_1^{(j)}, b_1^{(j)}, b_1^{(j)}, b_1^{(j)}) \\ (a_2^{(j)}, a_2^{(j)}, b_2^{(j)}, b_2^{(j)}, a_2^{(j)}, a_2^{(j)}, b_2^{(j)}, b_2^{(j)}) \\ (a_3^{(j)}, b_3^{(j)}, a_3^{(j)}, b_3^{(j)}, a_3^{(j)}, b_3^{(j)}, a_3^{(j)}, b_3^{(j)}) \end{matrix} \right\}. \tag{6}$$

For each level of membership, this produces 2^n combinations. For the highest level of membership, all combinations are equal to the core combination $(c_1, c_2, \ldots, c_n)$, so that only a single combination needs to be evaluated. For a problem with n parameters and $m+1$ intervals, this yields a set of $\mathcal{N}_{\mathrm{TM}}$ combinations, with

$$\mathcal{N}_{\mathrm{TM}} = 1 + m \cdot 2^n. \tag{7}$$

All these combinations are located on the $2^{(n-1)}$ diagonals (i.e. 2^n half-diagonals) of the hypercuboid in the parameter space that is spanned by the input vertex [11]. Fig. 3 shows an example adapted from Ref. [11], with three uncertain parameters (with symmetric triangular membership functions). The parameter combinations of the 5 interval levels are located on the $2^{(3-1)} = 4$ diagonals (i.e. $2^3 = 8$ half-diagonals) of the hypercuboid, which intersect at the core level.

The arrays $\hat{X}_i^{(j)}$ contain $1 + m \cdot 2^n$ parameter combinations. These combinations are evaluated via conventional arithmetic for crisp numbers, i.e. with deterministic, non-fuzzy computations. As proposed by Hanss [11], the deterministic outputs are stored in arrays $\hat{Z}^{(j)}$ that contain

$$\begin{aligned} (\text{for } j = 0, 1, \ldots, m-1), \quad & {}^k\hat{z}^{(j)}, \text{ the } k = 1..2^n \text{ outputs at the } j\text{th level} \\ (\text{for } j = m), \quad & \hat{z}^{(m)}, \text{ a single output at the core level.} \end{aligned} \tag{8}$$

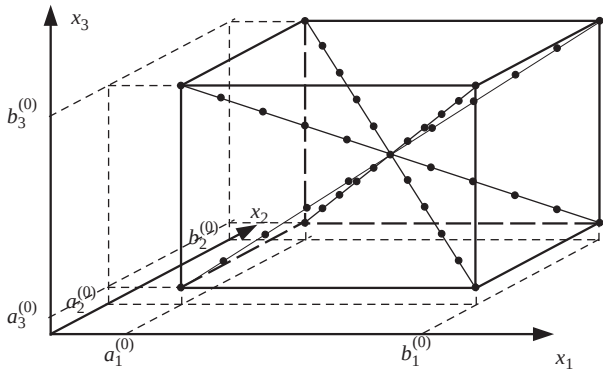

Fig. 3. Graphical representation of the Transformation Method in the parameter space (x_1, x_2, x_3), for $m = 5$. Each black dot is an evaluated parameter combination.

Subsequently, the interval representation $Z^{(j)} = [a^{(j)}, b^{(j)}]$, $j = 0, 1, ..., m$ of the fuzzy output q can be obtained via the repetitive procedure [11]

$$(\text{for } j = 0, 1, \ldots, m-1) \quad \begin{cases} a^{(j)} = \min\limits_{k} (a^{(j+1)},\ {}^{k}\hat{z}^{(j)}), \\ b^{(j)} = \max\limits_{k} (b^{(j+1)},\ {}^{k}\hat{z}^{(j)}), \end{cases} \tag{9}$$

$$(\text{for } j = m) \quad a^{(m)} = \hat{z}^{(m)} = b^{(m)}.$$

This means that the fuzzy output at the core level is equal to the single deterministic output at the core level. At a lower α-sublevel, the lower boundary $a^{(j)}$ of the fuzzy output's interval representation is the minimal value attained by ${}^{k}\hat{z}^{(j)}$ at a membership level $\mu_j \geqslant \alpha$. Equivalently, the upper boundary $b^{(j)}$ is the maximum value of ${}^{k}\hat{z}^{(j)}$ in the parameter range for which $\mu_j \geqslant \alpha$.

4. The Transformation Method in the frequency domain

In this paper, the TM is applied to visualize the effect of uncertain input parameters on the FRF characteristics of a structural FE model. Application of the TM to the frequency domain only requires that a frequency dimension is added to the output side of the procedure in Section 3. With a frequency increment Δf, the frequency range is given by $[f_{\min}, f_{\min} + \Delta f, \ldots, f_{\max}]$; this range of N_f samples is abbreviated as $[f_{\min}, f_{\max}]$ from here on. For the sake of completeness, the entire procedure in the frequency domain is summarized below.

The n uncertain input parameters are modelled as fuzzy numbers that are subdivided into $m + 1$ intervals (including the core level). The $\mathcal{N}_{\text{TM}} = 1 + m \cdot 2^n$ combinations of interval extrema are stored in the arrays $\hat{X}_i^{(j)}$, see Eq. (6). The combinations $\hat{X}_i^{(j)}$ are evaluated with deterministic computations, yielding FRF vectors ${}^{k}\hat{z}(f)^{(j)}$ instead of scalar outputs ${}^{k}\hat{z}^{(j)}$ as in Eq. (8). In analogy

with Ref. [11], the deterministic FRF vectors are stored in arrays $\hat{Z}(f)^{(j)}$ that contain

$$\begin{aligned} (\text{for } j = 0, 1, \ldots, m-1), \quad & {}^{k}\hat{z}(f)^{(j)}, \text{ the } k = 1..2^n \text{ FRFs at the } j\text{th level} \\ (\text{for } \ j = m), \quad & \hat{z}(f)^{(m)}, \text{ a single FRF at the core level.} \end{aligned} \tag{10}$$

The repetitive algorithm in Eq. (9) must be applied at each sampled frequency, yielding the interval representation of the fuzzy FRF amplitude at that frequency, given by

$$A^{(j)}(f) = [\underline{A}^{(j)}(f), \overline{A}^{(j)}(f)] \quad \text{for } j = 0, 1, \ldots, m \text{ and } f \in [f_{\min}, f_{\max}], \tag{11}$$

where $\underline{A}^{(j)}(f)$ and $\overline{A}^{(j)}(f)$ denote the lower and upper boundary of the fuzzy amplitude at the frequency f. Effectively, the amplitude at each sampled frequency is computed as an independent fuzzy number; for all frequencies combined, these amplitudes $A^{(j)}(f)$ form fuzzy envelopes at the $m+1$ levels of membership. At the highest level, the upper and lower envelopes are a single vector, namely the FRF vector at $\mu_j = 1$. At lower interval levels $\mu_j = \alpha$, the lower envelope is the vector of minimal amplitude values attained by the deterministic FRF vectors for membership levels $\mu_j \geqslant \alpha$; equivalently, the upper envelope is the vector of maximal amplitude values attained by the deterministic FRF vectors for $\mu_j \geqslant \alpha$.

4.1. Note on the applicability

The TM has been presented by Hanss as a practical implementation of fuzzy arithmetic, yielding "the proper—and in case of non-monotonic problems at least nearly proper—results". This is quite logical: when a function $f(X)$ depends monotonically on its n input parameters $x_1, x_2, \ldots, x_n$, the extreme values of the function value $f(X)$ are always found on the combinations of the input vertex extrema; for the example in Fig. 3, this corresponds to the corner points of the hypercuboid. For a monotonic function $f(X)$, the TM can be used with $m = 1$ in order to assess the full range of the output uncertainty.

As a fuzzy FRF is a sequence of fuzzy amplitudes, the TM requires that the *amplitude magnitudes* at each sampled frequency depend on the input parameters in a monotonic way. This is often not the case: as mentioned in the introduction, it are often the *eigenfrequency values* of a structure that depend on global input parameters (mass density, Young's modulus, shell thickness, etc.) in a monotonic way. For the FRF of such a structure, consider a frequency sample f that lies just above a resonance frequency f_R. When a parameter change Δx is applied, the resonance frequency f_R might shift toward the sampled frequency f, so that the amplitude $A(f)$ increases. When a larger parameter change is applied, the resonance frequency f_R may pass through the sampled frequency f, resulting in a decrease of the amplitude $A(f)$ as a result of the parameter change. The amplitude at a given frequency is then clearly not monotonic in x. As has previously been demonstrated in [14], the non-monotonicity of the FRF amplitudes and the TM's sampling procedure cause an undesired effect, namely a saw-like shape of the TM envelope: some resonance peaks are simply "missed" by the deterministic computations. With a sufficiently high number of membership levels (typically between 5 and 10, depending on the dynamic structure and the range of the input uncertainty), the size of these saw-teeth is limited and the TM's FRF envelopes are sufficiently accurate. In other words, one needs enough "intermediate deterministic FRFs" to reconstruct the entire fuzzy FRF. Note that any engineer can recognize the saw-teeth

and choose to ignore them. This effect therefore does not limit practical applications, as will be demonstrated in Sections 8 and 9.

The number of interval levels m may result in a high computation time for the TM, as a number of $\mathcal{N}_{\mathrm{TM}} = 1 + m \cdot 2^n$ deterministic computations is required. It is very important to reduce the number of computations required for an uncertainty assessment. For this purpose, the Short Transformation Method (STM) is proposed in the next section.

5. The Short Transformation Method

5.1. Outline of the Short Transformation Method

The STM is presented as a cost-effective alternative to the original TM [11] for frequency-domain applications, allowing to reconstruct the fuzzy FRF from a much lower number of deterministic computations with only a small reduction in the accuracy. The STM is based on the assumption that a single diagonal in the parameter space (i.e. 2 half-diagonals) is sufficient to assess FRF uncertainty. The STM's DOE has been visualized in Fig. 4; the procedure is summarized as follows:

(1) Compute an initial set of FRF vectors, at the input vertex combinations (at $\mu = 0$) and at the core combination x_c.
(2) Identify the *principal diagonal*, i.e. the diagonal in the parameter space that has the largest contribution to the shape of the FRF envelope, from the initial set of FRF vectors.
(3) Evaluate only the 2 parameter combinations on the principal diagonal for the remaining levels of membership (with m typically between 5 and 10, as with the TM).

When comparing Figs. 3 and 4, it is clear that the proposed STM leads to a large reduction of the number of experiments with respect to the original TM. The STM requires a number of

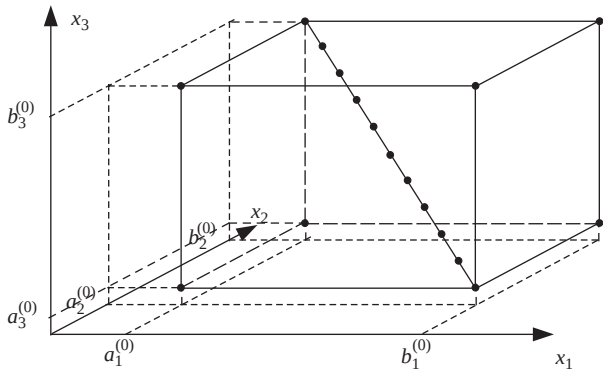

Fig. 4. Graphical representation of the STM in the parameter space (x_1, x_2, x_3), for $m = 5$. Each black dot represents an evaluated parameter combination.

computations $\mathcal{N}_{\mathrm{STM}}$, given by

$$\mathcal{N}_{\mathrm{STM}} = 1 + 2^n + 2 \cdot (m-1). \tag{12}$$

The reduction number is then equal to $2^{n-1} \cdot (m-1)$, i.e. the difference between $\mathcal{N}_{\mathrm{TM}}$ in Eq. (7) and $\mathcal{N}_{\mathrm{STM}}$ in Eq. (12); the reduction percentage increases exponentially with the number of inputs. In analogy with Ref. [11] and Section 4, the FRF vectors that result from the $\mathcal{N}_{\mathrm{STM}}$ deterministic computations are stored in arrays $\hat{Z}(f)^{(j)}$ that contain

$$\begin{array}{ll} (\text{for } j=0) & {}^{k}\hat{z}(f)^{(0)}, \text{ the } k = 1..2^n \text{ FRFs at the 0th level} \\ (\text{for } j=1,2,\ldots,m-1) & {}^{k}\hat{z}(f)^{(j)}, \text{ the } k = 1..2 \text{ FRFs at the } j\text{th level} \\ (\text{for } j=m) & \hat{z}(f)^{(m)}, \text{ a single FRF at the core level.} \end{array} \tag{13}$$

Again, the repetitive procedure in Eq. (9) is applied at each sampled frequency f, in order to find the interval representation of the fuzzy FRF amplitudes $A^{(j)}(f)$ as given in Eq. (11).

Note that the regularity of the TM's DOE allows easy identification of the parameter pairs that span the diagonals in the parameter space. Each parameter combination at index $k = 1..2^n$ on the input vertex has an opposite combination at index $2^n + 1 - k$; these indices correspond to the columns of $\hat{X}_i^{(j)}$, see for example the columns of Eq. (6). For each of the FRF vectors ${}^{k}\hat{z}(f)^{(0)}$ that are computed for the $k = 1..2^n$ parameter combinations on the input vertex in Eq. (13), the FRF vector on the opposite side of the input vertex is therefore given by ${}^{2^n+1-k}\hat{z}(f)^{(0)}$.

5.2. Assumptions for the STM

The STM assumes that for the structure under consideration, a parameter change results in (more or less) monotonic changes of the eigenfrequency values. As an example, Fig. 5 shows the frequency response of a single degree of freedom (dof) system. At the single eigenfrequency, the FRF attains its single resonance peak.

Suppose that the structure has a single uncertain input $x \in [x_{\min}, x_{\max}]$, and that an eigenfrequency f_c is obtained at the core x_c. When the frequency f depends on the input x in a monotonic way, an input increase dx results in an increase df of the eigenfrequency magnitude.

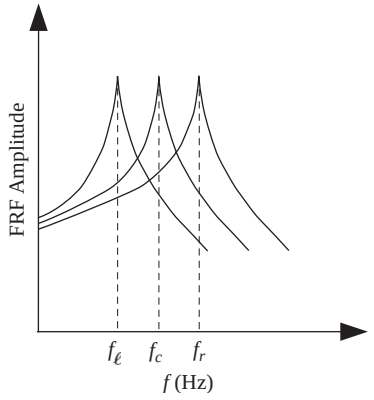

Fig. 5. Example: FRF with a single resonance peak, subject to monotonic shifts.

The highest eigenfrequency magnitude f_r is then obtained at $x_{\max}$, yielding the FRF that lies most to the right-hand side of the frequency range. Vice versa, the lowest eigenfrequency magnitude f_ℓ, yielding the FRF most to the left, is found at $x_{\min}$.

In general, consider a structure with an input vector X, for which an FRF is computed in a range with more than one eigenfrequency. When each eigenfrequency depends on the input vector in a monotonic way, one can expect that there exists a pair of parameter combinations on the input vertex with the *largest contribution to the global FRF envelope*: a parameter combination X_{left} will have the largest contribution to the *left-hand side* of the global FRF envelope, and the opposite parameter combination X_{right} will have the largest contribution to the *right-hand side* of the global FRF envelope. This pair of parameter combinations is located on the same *diagonal* in the parameter space, denoted as *principal diagonal* from here on. This can be illustrated on the basis of Fig. 4. Assume that $X_{\text{left}} = (a_1^{(0)}, b_2^{(0)}, b_3^{(0)})$ has the largest influence on the left-hand side of the FRF envelope. The opposite combination $X_{\text{right}} = (b_1^{(0)}, a_2^{(0)}, a_3^{(0)})$ then lies on the same diagonal in the parameter space. When parameter changes induce monotonic eigenfrequency shifts, X_{right} will produce the FRF vector with the largest contribution to the right-hand side of the global FRF envelope. The next section proposes a method to identify the principal diagonal.

5.3. Heuristic procedure to select the principal diagonal

The core of the STM is a *heuristic procedure* to select the principal diagonal from the initial set of FRF vectors. In this section, the successive steps of the heuristic procedure are given, illustrated on the basis of a simplified set of FRF vectors.

5.3.1. Find global envelope of the initial FRF data

When the FRF vectors have been computed for the initial $2^n + 1$ parameter combinations, the global envelope $A_g^0(f)$ of these FRF vectors is given by

$$A_g^0(f) = [\underline{A}^0(f), \overline{A}^0(f)] \quad \text{for } f \in [f_{\min}, f_{\max}], \tag{14}$$

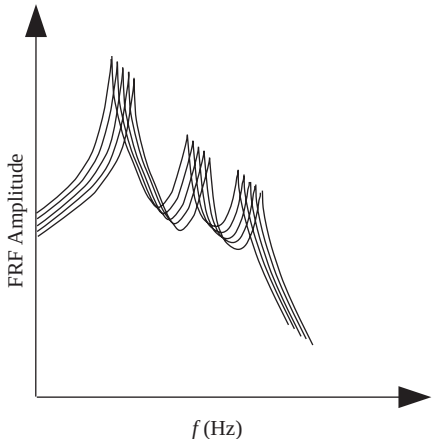

Fig. 6. Illustration example for the Short Transformation Method: a set of five FRF vectors.

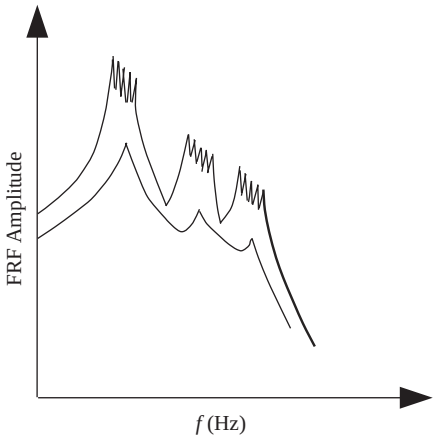

Fig. 7. The global FRF envelope $A_g^0(f)$ of the FRF vector set in Fig. 6.

where $\underline{A}^0(f)$ and $\overline{A}^0(f)$ denote the lower and upper boundary, respectively, of the FRF amplitude at the frequency f. Fig. 6 shows an example set of 5 FRF vectors, that have the global envelope $A_g^0(f)$ shown in Fig. 7.

5.3.2. Find characteristic segments on the left- and right-hand side

The 2^n parameter combinations on the input vertex can be ordered in 2^{n-1} pairs with opposite properties; the 2^{n-1} diagonals (i.e. 2^n half-diagonals) in the parameter space are spanned by these pairs. This section proposes an approach to identify the pair $[X_{\text{left}}, X_{\text{right}}]$ that spans the principal diagonal in the parameter space from the global FRF envelope $A_g^0(f)$ in Eq. (14). Recall Figs. 6 and 7, that show the example set of FRF vectors and the global envelope $A_g^0(f)$ of the set, respectively. Fig. 8 shows the FRF vectors with the largest contribution to the left- and right-hand side of the global FRF envelope, respectively. These FRF vectors, that are denoted as *left FRF* and *right FRF* vector from here on, are attained at parameter values X_{left} and X_{right}, respectively. By comparing Figs. 7 and 8, it can be seen that

- the *left FRF* vector has a large shape conformity with the *ascending line segments of the upper envelope* $\overline{A}^0(f)$ and with the *descending line segments of the lower envelope* $\underline{A}^0(f)$
- the *right FRF* has a large shape conformity with the *descending line segments of the upper envelope* $\overline{A}^0(f)$ and with the *ascending line segments of the lower envelope* $\underline{A}^0(f)$

provided that only line segments with a sample length above a certain threshold are considered. Based on this notion, an algorithm has been designed to find the *characteristic segments* $L_i \in \mathscr{L}$ and $R_j \in \mathscr{R}$ that are expected to have a large shape conformity with the left and right FRF, respectively; Fig. 9 shows these segments for the example set. The left and right FRF vectors, attained at parameter combinations X_{left} and X_{right} that span the principal diagonal, are found as the best matches with these characteristic segments.

First, the numerical derivatives of the upper global envelope $\overline{A}^0(f)$ and the lower global envelope $\underline{A}^0(f)$ are computed at each frequency sample f, using the forward finite difference

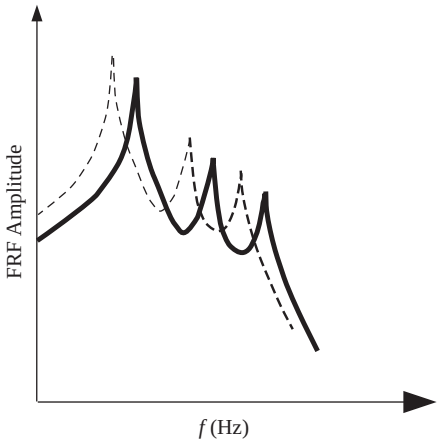

Fig. 8. The left FRF vector (dashed line) and the right FRF vector (solid line) of the FRF vector set in Fig. 6.

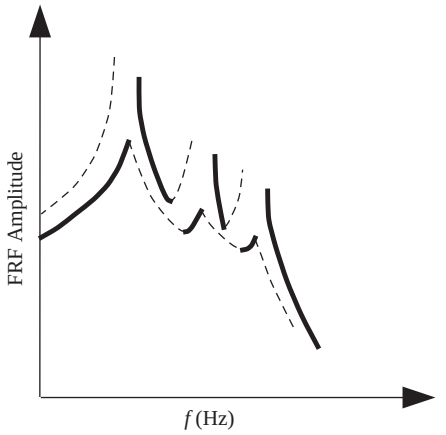

Fig. 9. The characteristic segments of the left-hand side (dashed lines) and right-hand side (solid lines) of the global envelope $A_g^0(f)$ in Fig. 7.

(FFD) approximation [15]

$$\frac{\partial \overline{A}^0}{\partial f}(f) \approx \frac{\overline{A}^0(f+\Delta f) - \overline{A}^0(f)}{\Delta f} \quad \text{for} \quad f \in [f_{\min}, f_{\min}+\Delta f, \ldots, f_{\max}-\Delta f],$$
$$\frac{\partial \underline{A}^0}{\partial f}(f) \approx \frac{\underline{A}^0(f+\Delta f) - \underline{A}^0(f)}{\Delta f}. \tag{15}$$

In addition, a set of counters is used to monitor the ascending/descending length of the line segments of the global FRF envelope $A_g^0(f)$:

- $\mathscr{I}_{U,\mathrm{as}}(f)$ denotes the frequency segment length for which the *upper FRF envelope* $\overline{A}^0(f)$ *is ascending* at a frequency f;

- $\mathscr{I}_{U,\mathrm{de}}(f)$ denotes the frequency segment length for which the *upper FRF envelope* $\overline{A}^0(f)$ *is descending* at a frequency f;
- $\mathscr{I}_{L,\mathrm{as}}(f)$ denotes the frequency segment length for which the *lower FRF envelope* $\underline{A}^0(f)$ *is ascending* at a frequency f;
- $\mathscr{I}_{L,\mathrm{de}}(f)$ denotes the frequency segment length for which the *lower FRF envelope* $\underline{A}^0(f)$ *is descending* at a frequency f.

As an example, the counter $\mathscr{I}_{U,\mathrm{as}}(f)$ is initialized as $\mathscr{I}_{U,\mathrm{as}}(f_{\min})=0$; for frequency samples $f>f_{\min}$, the counter is updated as follows:

$$\mathscr{I}_{U,\mathrm{as}}(f)=\begin{cases}\mathscr{I}_{U,\mathrm{as}}(f-\Delta f)+1 & \text{if } \dfrac{\partial\overline{A}^0}{\partial f}(f)>0,\\ 0 & \text{if } \dfrac{\partial\overline{A}^0}{\partial f}(f)\leqslant 0.\end{cases} \tag{16}$$

The gradient values and the counters are then used to filter the characteristic line segments from the global envelope

- A *threshold* $\mathscr{T}$ is introduced as *the minimal length of the ascending and descending characteristic line segments*. A line segment with a length below the threshold is not considered; if the length is above the threshold, the *entire line segment* is considered. The threshold is a user-defined parameter that must be tuned to filter out the short line segments. This is necessary in order to neglect the short segments around the resonance peaks (see e.g. Fig. 7), that should not be used to identify the left and right FRF.
- As FRF characteristics are not always as clean as in Fig. 9, frequencies may exist where both the upper and lower line segment belong to an envelope side. For example, if the upper envelope is ascending and the lower envelope is descending simultaneously at a frequency f, both line segments could belong to the set of characteristic segments on the left-hand side. This is undesirable, as it roughens the shape of the characteristic segments, which deteriorates the identification on the basis of Eq. (17) later on. The line segment with the largest length at the frequency f is kept in such case; the shortest segment is ignored.

For a given threshold, one thus obtains the *characteristic segment sets* $\mathscr{L}=[L_1,L_2,\ldots,L_N]$ on the left-hand side and $\mathscr{R}=[R_1,R_2,\ldots,R_M]$ on the right-hand side of the global envelope, as in the example in Fig. 9.

5.3.3. Locate the principal diagonal

To locate the principal diagonal, the parameter pair on the input vertex must be selected that yields the two FRF vectors with the highest shape conformity with the characteristic segment sets on the left- and right-hand side, respectively. As a shape conformity factor, the Variance Accounted For (VAF) is used [16], that is defined between a reference vector y and

its estimate $\hat{y}$ as

$$\mathscr{V}(y,\hat{y}) = \left(1 - \frac{\mathrm{var}(y-\hat{y})}{\mathrm{var}(y)}\right)100\%, \tag{17}$$

where var(y) is the variance of y, given by $E\{[y - E\{y\}]^2\}$. The VAF can attain values between $-\infty$ (if there is no shape conformity at all) and 100% (if y and $\hat{y}$ are identical vectors).

As each of the $k = 1..2^n$ parameter combinations on the input vertex has an opposite combination at an index $2^n + 1 - k$, the shape conformity of each FRF pair with the left and right FRF characteristics can be quantified by computing the so-called VAF sums $\mathscr{V}_{\mathrm{sum}}(k)$

$$\mathscr{V}_{\mathrm{sum}}(k) = \frac{\mathscr{V}(\mathscr{L}, {}^{k}\hat{z}(f)^{(0)}) + \mathscr{V}(\mathscr{R}, {}^{2^n+1-k}\hat{z}(f)^{(0)})}{2} \quad \text{for } k = 1..2^n. \tag{18}$$

For each of these computations, the vectors ${}^{k}\hat{z}(f)^{(0)}$ are reduced to the frequency samples where $\mathscr{L}$ and $\mathscr{R}$ have non-zero values (i.e. where the characteristic line segments are defined), as this improves the selection based on the VAF sums $\mathscr{V}_{\mathrm{sum}}(k)$ in Eq. (18). The principal diagonal is identified as the parameter pair $[X_{\mathrm{left}}, X_{\mathrm{right}}]$ at the position $(k, 2^n + 1 - k)$ for which $\mathscr{V}_{\mathrm{sum}}(k)$ attains a maximal value. Two checks are used to assess the correctness of the obtained solution:

- the maximal value of the $\mathscr{V}_{\mathrm{sum}}(k)$ can be compared with the second-largest value of the $\mathscr{V}_{\mathrm{sum}}(k)$; if there is indeed a single diagonal with a large contribution to the left- and right-hand side, one can expect that this difference is substantial;
- when the maximal value of $\mathscr{V}_{\mathrm{sum}}(k)$ is obtained at the parameter combination $(k, 2^n + 1 - k)$, one can expect to find a very low value of $\mathscr{V}_{\mathrm{sum}}(2^n + 1 - k)$ at the opposite parameter combination $(2^n + 1 - k, k)$. This can be understood from Fig. 8: the FRF with the largest shape conformity on the left-hand side has almost no shape conformity with the right-hand side of the global envelope, and vice versa.

When the principal diagonal has been identified with the described heuristic procedure, the STM can be executed as described in Section 5.1.

6. Results validation criteria

The TM and STM envelopes are validated against FRF data from a sufficiently large number N_{mc} of Monte Carlo (MC) simulations, with a uniform distribution in the problem's input vertex, in order to randomly sample all *possible* input parameter combinations. Recall that the fuzzy FRF envelopes of the TM and STM have the form $A^{(j)}(f)$ in Eq. (11); from here on, the lower and upper global envelopes of TM and STM are given by $[\underline{A}^{(0)}_{\mathrm{TM}}(f), \overline{A}^{(0)}_{\mathrm{TM}}(f)]$ and $[\underline{A}^{(0)}_{\mathrm{STM}}(f), \overline{A}^{(0)}_{\mathrm{STM}}(f)]$, respectively. In analogy with Eqs. (10) and (11), the Monte Carlo FRF vectors are stored in arrays ${}^{k}\hat{z}_{\mathrm{MC}}(f)$, for $k = 1..N_{\mathrm{mc}}$, that have a global FRF envelope $A_{\mathrm{MC}}(f) = [\underline{A}_{\mathrm{MC}}(f), \overline{A}_{\mathrm{MC}}(f)]$.

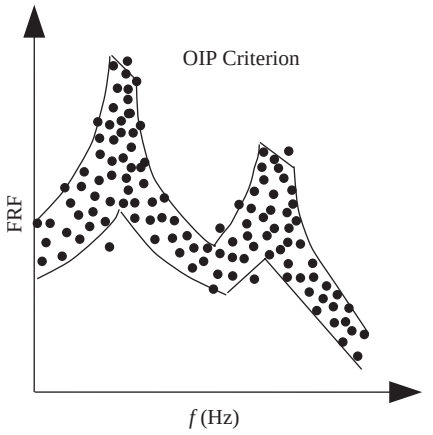

Fig. 10. The *overall inclusion percentage* (OIP) is the percentage of Monte Carlo FRF data samples that lie between the (Short) Transformation Method envelopes (black solid lines).

6.1. First validation criterion: Overall inclusion percentage

The overall inclusion percentage (OIP) is the first validation criterion, that denotes the percentage of Monte Carlo FRF samples that lies between the global envelopes of the TM (or, equivalently, of the STM). This requires that an indicator flag $\mathscr{I}(f,k)$ is introduced for each of the FRF vectors ${}^{k}\hat{z}_{\mathrm{MC}}(f)$, for $k = 1..N_{\mathrm{mc}}$

$$\mathscr{I}(f,k) = \begin{cases} 1 & \text{if } \underline{A}^{(0)}_{\mathrm{TM}}(f) \leqslant {}^{k}\hat{z}(f)_{\mathrm{MC}} \leqslant \overline{A}^{(0)}_{\mathrm{TM}}(f), \\ 0 & \text{otherwise.} \end{cases} \tag{19}$$

The inclusion percentage $\mathrm{IP}(f)$ at sampled frequencies $f \in [f_{\min}, f_{\max}]$ is then given by

$$\mathrm{IP}(f) = \left(\frac{1}{N_{\mathrm{mc}}} \sum_{k=1}^{N_{\mathrm{mc}}} \mathscr{I}(f,k) \right) 100\%. \tag{20}$$

The overall inclusion percentage (OIP, see Fig. 10) is then obtained as the average of $\mathrm{IP}(f)$ in the frequency range $[f_{\min}, f_{\max}]$:

$$\mathrm{OIP} = \frac{1}{N_f} \sum_{f=f_{\min}}^{f_{\max}} \mathrm{IP}(f). \tag{21}$$

6.2. Second validation criterion: Variance accounted for

Recall the VAF in Eq. (17), the shape conformity factor $\mathscr{V}(y,\hat{y})$ between a reference vector y and its estimate $\hat{y}$ [16]:

$$\mathscr{V}(y,\hat{y}) = \left(1 - \frac{\mathrm{var}(y-\hat{y})}{\mathrm{var}(y)} \right) 100\%.$$

The VAF criterion (see Fig. 11) is used to compare the upper and lower Monte Carlo envelopes, $\overline{A}_{\mathrm{MC}}(f)$ and $\underline{A}_{\mathrm{MC}}(f)$, with the global envelopes of TM and STM, respectively. The Monte Carlo

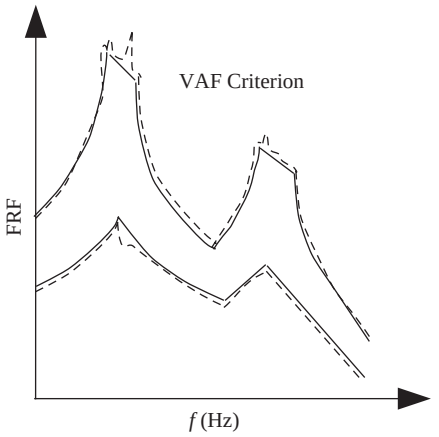

Fig. 11. The *variance accounted for* (VAF) criterion is a shape conformity factor between the upper and lower envelopes of the (Short) TM (solid lines) and the Monte Carlo envelopes (dashed lines).

envelopes are taken as reference vectors y, the TM and STM envelopes are considered as estimates $\hat{y}$ in Eq. (17).

- For the TM, this yields upper and lower VAF values $\mathscr{V}^{\text{up}}_{\text{TM}}(\overline{A}_{\text{MC}}(f), \overline{A}_{\text{TM}}(f))$ and $\mathscr{V}^{\text{lo}}_{\text{TM}}(\underline{A}_{\text{MC}}(f), \underline{A}_{\text{TM}}(f))$;
- for the STM, this yields upper and lower VAF values $\mathscr{V}^{\text{up}}_{\text{STM}}(\overline{A}_{\text{MC}}(f), \overline{A}_{\text{STM}}(f))$ and $\mathscr{V}^{\text{lo}}_{\text{STM}}(\underline{A}_{\text{MC}}(f), \underline{A}_{\text{STM}}(f))$.

7. Implementation

In Sections 8 and 9, two FE models are introduced as example structures for uncertainty assessment, for which uncertain inputs and an FRF vector of interest are defined. The effect of the input uncertainty on the FRF characteristics is then assessed with both TM and STM, and validated against Monte Carlo simulations.

The algorithms have been implemented in MATLAB [17]. Process management is performed with OPTIMUS [18], that launches the deterministic computations for the required parameter combinations and collects the results. Each deterministic computation is performed with an MSC/NASTRAN [19] Modal Frequency Response case (SOL 111). First, the modal contributions are computed in the frequency range of interest; modal superposition is then used to obtain the deterministic FRF amplitude vectors.

8. Analysis of a clamped plate

8.1. Problem definition

The first test structure is a clamped plate of $0.5 \times 0.35\,\text{m}^2$ in the x, y-plane, consisting of 441 nodes and 400 elements (i.e. a 20×20 element mesh). The plate has been clamped along the

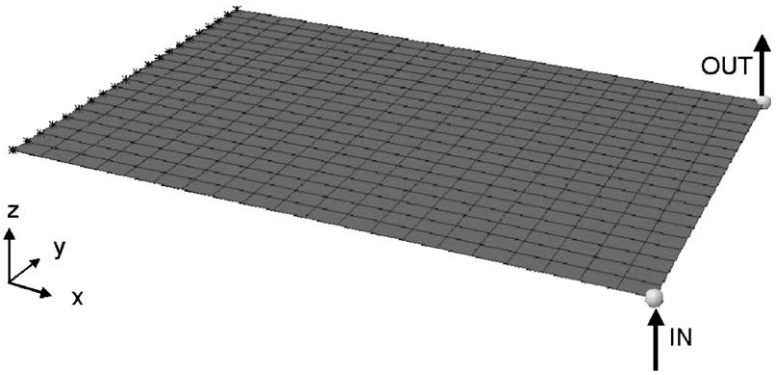

Fig. 12. Example 1: a thin plate in the x, y-plane, clamped along the left-hand side. The w/F FRF characteristics are computed between dof "IN" and "OUT" in the figure, both in the $+z$-direction.

Table 1
Uncertain input parameters of the clamped plate in Fig. 12

	Parameter X_i (unit)	Input range $[X_{\min}, X_{\max}]$	Core value X_c
X_1	Young's modulus (10^9 N/m^2)	[200, 220]	210
X_2	Mass density (kg/m^3)	[7600, 8000]	7800
X_3	Shell thickness (10^{-3} m)	[2, 3]	2.5

y-axis, as can be seen in Fig. 12 [20]. The FRF is defined between the input dof (force F applied in direction $+z$) at the lower right corner and the output dof (displacement w in direction $+z$) at the upper right corner. For this plate, the shell thickness, mass density and Young's modulus are introduced as uncertain parameters that are modelled as symmetric triangular membership functions with the range and the core as defined in Table 1. Modal damping has been set to 1% for all modes. For each deterministic FRF computation, the modes have been computed in the frequency range $[0, 300]$ Hz. Modal superposition then yields the FRF vector in the range $[0, 200]$ Hz with an increment of 1 Hz. This example has previously been analysed with the TM in [14].

8.2. Results with the Transformation Method

For the clamped plate with the $n = 3$ uncertain parameters in Table 1, the number of interval levels is set to $m = 10$, so that the TM requires a number of $\mathcal{N}_{\mathrm{TM}} = 1 + m \cdot 2^n = 81$ deterministic experiments. Using Eq. (13), the fuzzy FRF in Fig. 13 has been obtained from the set of deterministic FRF vectors.

8.3. Results with the Short Transformation Method

The FRF of the clamped plate has then been estimated with the STM. As described in Section 5.3, an initial DOE is performed on the input vertex and at the core combination, to obtain the

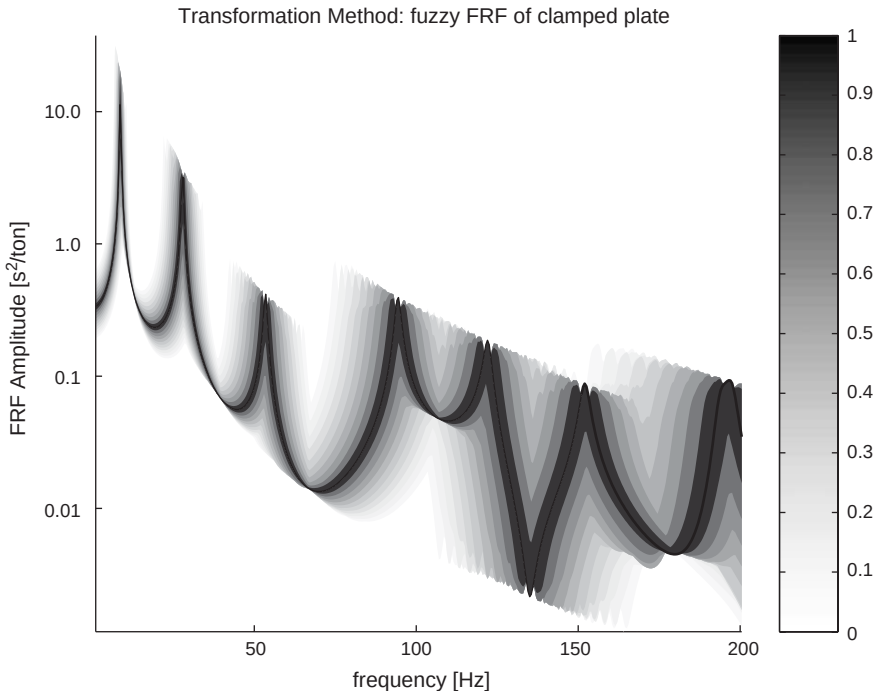

Fig. 13. Fuzzy FRF of the clamped plate in Fig. 12, obtained with the transformation method in the range 0–200 Hz. A darker colour represents a higher level of membership of the fuzzy FRF output.

initial FRF $A_g^0(f)$ in Eq. (14). The threshold $\mathscr{T}$ for the length of the left and right segments $\mathscr{L}$ and $\mathscr{R}$ has been set to 8. With the $\mathscr{V}_{\text{sum}}(k)$ in Eq. (18) it has then been found that the principal diagonal is spanned by the parameter pair $[X_{\text{left}}, X_{\text{right}}]$ at the indices $(k, 2^n + 1 - k) = (4, 5)$ on the TM's DOE; this corresponds to columns 4 and 5 of Eq. (6); X_{left} is thus found at $(a_1^{(0)}, b_2^{(0)}, b_3^{(0)})$ and X_{right} at $(b_1^{(0)}, a_2^{(0)}, a_3^{(0)})$. The following selection criteria for the principal diagonal have been found:

- The maximal value of $\mathscr{V}_{\text{sum}}(k)$ is attained at $k = 4$: $\mathscr{V}_{\text{sum}}(4) = 75.6\%$.
- The second highest value of $\mathscr{V}_{\text{sum}}(k)$ is attained at $k = 3$: $\mathscr{V}_{\text{sum}}(3) = 64.4\%$.
- For the selected principal diagonal, the opposite combination $(5, 4)$ yields a very low value of $\mathscr{V}_{\text{sum}}(5) = -233.6$.

For higher levels of membership, only the two parameter combinations on the principal diagonal have been evaluated, i.e. $(a_1^{(j)}, b_2^{(j)}, b_3^{(j)})$ and $(b_1^{(j)}, a_2^{(j)}, a_3^{(j)})$ for $j = 2..m$, yielding $2 \cdot (m - 1) = 18$ additional deterministic experiments. The total number of deterministic computations performed by the STM is therefore equal to $\mathscr{N}_{\text{STM}} = 1 + 2^n + 2 \cdot (m - 1) = 27$. For the obtained set of deterministic FRF vectors, Eq. (13) has been used to reconstruct the fuzzy FRF, which is shown in Fig. 14.

In Section 8.5, the results with the STM are given for other diagonal selections than the principal diagonal. For this purpose, note that the third highest value of $\mathscr{V}_{\text{sum}}(k)$ is attained at

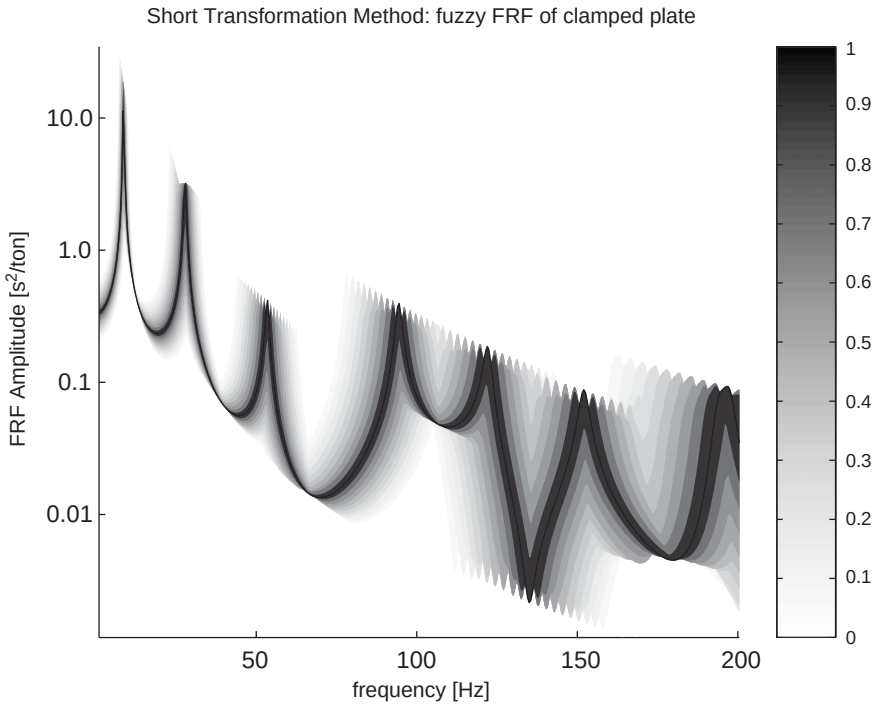

Fig. 14. Fuzzy FRF of the clamped plate in Fig. 12, obtained with the Short Transformation Method in the range 0–200 Hz. A darker colour represents a higher level of membership of the fuzzy FRF output.

$k = 1$ ($\mathscr{V}_{\text{sum}}(1) = 63.6\%$), and the fourth highest value at $k = 2$ ($\mathscr{V}_{\text{sum}}(2) = 46.9\%$). After the initial DOE, the 4 diagonals can thus be ranked as follows: the principal diagonal at combination $(4, 5)$ on the input vertex yields the highest $\mathscr{V}_{\text{sum}}(k)$, followed by diagonals at combinations $(3, 6)$, $(1, 8)$ and finally $(2, 7)$.

8.4. Validation and assessment

The FRF data samples of $\mathscr{N}_{\text{MC}} = 500$ Monte Carlo simulations, uniformly distributed over the input vertex (i.e. the Input range in Table 1), are used to validate the fuzzy FRF of the TM and the STM, respectively, with the criteria defined in Section 6. The results are given in Table 2. Clearly, the STM is more effective than the TM, as it reduces the number of experiments with a factor 3, with only a very slight loss of accuracy.

Fig. 15 partly shows the upper envelopes of Monte Carlo (thick, grey), TM (medium thickness) and STM (thin) in a single figure. Note the following:

- As the STM's DOE is a subset of the TM's DOE, the global envelope of the STM never exceeds the envelope of the TM.
- The TM envelope has a saw-like shape, as a result of the limited sampling plan. The saw-teeth of the STM envelope are somewhat deeper, but the actual envelope shape can still be

Table 2
Clamped plate: validation of TM and STM envelopes against Monte Carlo data

Transformation Method $\mathcal{N}_{TM} = 81$ experiments	Short Transformation Method $\mathcal{N}_{STM} = 27$ experiments
$OIP_{TM} = 98.3\%$ $\mathcal{V}^{up}_{TM}(\overline{A}_{MC}(f), \overline{A}_{TM}(f)) = 97.9\%$ $\mathcal{V}^{lo}_{TM}(\underline{A}_{MC}(f), \underline{A}_{TM}(f)) = 99.5\%$	$OIP_{STM} = 96.2\%$ $\mathcal{V}^{up}_{STM}(\overline{A}_{MC}(f), \overline{A}_{STM}(f)) = 97.2\%$ $\mathcal{V}^{lo}_{STM}(\underline{A}_{MC}(f), \underline{A}_{STM}(f)) = 99.4\%$

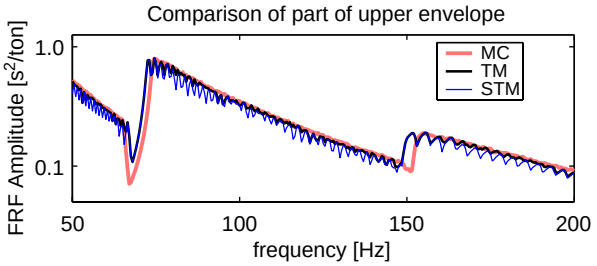

Fig. 15. Envelope comparison: The upper FRF envelope obtained with Monte Carlo (thick, grey), TM (thick, black, from Fig. 13) and STM (thin, black, from Fig. 14) in the range 50–200 Hz.

recognized. The Monte Carlo has a smooth shape, as many intermeditate resonance peaks have been sampled.

- The Monte Carlo method is not an ideal reference, as even a high number of samples cannot prevent that vertex combinations are missed. For example, the set of 500 Monte Carlo FRF vectors does not contain the most left FRF around 150 Hz, that has been located with the TM and STM.

8.5. *Justification of the proposed diagonal selection*

For simple structures, one can argue to select the principal diagonal based on physical considerations. The clamped plate only has bending modes; the lowest eigenfrequencies are attained at the minimum of the Young's modulus, the maximum of the mass density and the minimum of the shell thickness [12]; the highest eigenfrequency values at the opposite extrema. When one selects the left and right FRF based on this reasoning, one selects $X_{left} = (a_1^{(0)}, b_2^{(0)}, a_3^{(0)})$ and $X_{right} = (b_1^{(0)}, a_2^{(0)}, b_3^{(0)})$, the vertex pair with the second-highest $\mathcal{V}_{sum}(k)$ of 64.4%. Note that such a simple reasoning cannot be followed for a structure of arbitrary complexity. The advantage of the proposed selection method is that it is only based on the FRF data at the initial DOE.

This section aims to justify the proposed selection method of the principal diagonal, by repeating the analysis in Sections 8.3 and 8.4 for other diagonals than the principal diagonal. The uncertain FRF predictions with the STM are validated in this section with the criteria introduced

Table 3
Comparison of STM predictions of the clamped plate FRF, for all 4 diagonals that can be selected

Selected diagonal, at combination (...,...)	$\mathscr{V}_{\text{sum}}(k)$ (ranking)	Validation criteria (ranking)		
		OIP	VAF $\mathscr{V}^{\text{up}}$	VAF $\mathscr{V}^{\text{lo}}$
(4, 5), i.e. principal diagonal	75.6% (1)	96.2% (1)	97.2% (1)	99.5% (1)
(3, 6)	64.4% (2)	96.0% (3)	97.1% (2)	99.4% (3)
(1, 8)	63.6% (3)	95.9% (4)	95.5% (3)	99.4% (3)
(2, 7)	46.9% (4)	96.1% (2)	94.7% (4)	99.5% (1)

The results and ranking based on the $\mathscr{V}_{\text{sum}}(k)$ criterion are compared with the results and ranking based on the OIP and VAF, i.e. the validation criteria of the fuzzy FRF against Monte Carlo data.

in Section 6. Table 3 compares the ranking according to these validation criteria with the ranking according to the $\mathscr{V}_{\text{sum}}(k)$ (see Section 8.3). It can be seen that the principal diagonal, predicted from the $\mathscr{V}_{\text{sum}}(k)$ ranking, yields the best results on all validation criteria. For the other diagonals, the rankings based on $\mathscr{V}_{\text{sum}}(k)$ and the validation criteria are clearly correlated.

9. Analysis of a car front cradle

9.1. Problem definition

The second test structure is a car front cradle, a stiff framework that is attached to the car body to support the engine in the car and to provide attachment points for the suspension arms. Fig. 16 [20] shows the FE model, that consists of 1934 nodes and 2221 elements.

The structure has been clamped rigidly at the 4 connection points to the car body; i.e. a rigid coupling is assumed. The FRF is defined between the input dof (force F applied in direction $+z$) at one of the engine mounts (where the engine is connected to the front cradle) and the output dof (displacement w in direction $+z$) on the top beam. The shell thickness, mass density and Young's modulus have been introduced as uncertain parameters that are modelled as symmetric triangular membership functions with the range and the core as defined in Table 4. Modal damping of 1% has been set for all modes. For each deterministic FRF computation, the modes have been computed in the frequency range [0, 2000] Hz. Modal superposition then yields the FRF in the range [100, 1100] Hz with an increment of 1 Hz. This analysis case has previously been reported in [14].

9.2. Results with the Transformation Method

For the car front cradle with the $n = 3$ uncertain parameters in Table 4, the number of interval levels is set to $m = 10$, so that the TM again requires $\mathscr{N}_{\text{TM}} = 1 + m \cdot 2^n = 81$ deterministic experiments. Eq. (13) has been used to obtain the fuzzy FRF in Fig. 17 from the set of deterministic FRF vectors.

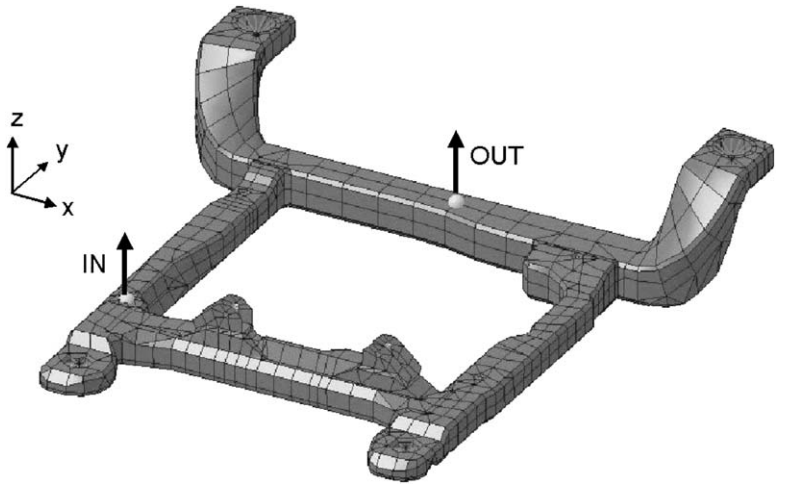

Fig. 16. Example 2: a car front cradle, rigidly clamped at the 4 connection points to the car body. The w/F FRF characteristics are computed between dof "IN" and "OUT" in the figure, both in the $+z$-direction.

Table 4
Uncertain input parameters of the car front cradle in Fig. 16

	Parameter X_i (unit)	Input range $[X_{\min}, X_{\max}]$	Core value X_c
X_1	Young's modulus (10^9 N/m^2)	[190, 210]	200
X_2	Mass density (kg/m^3)	[7600, 8000]	7800
X_3	Shell thickness (10^{-3} m)	[1.6, 2.4]	2.0

9.3. Results with the Short Transformation Method

The FRF of the car front cradle has been estimated also with the STM. Again, an initial DOE is performed on the input vertex and at the core combination, to obtain the initial FRF envelope $A_g^0(f)$ in Eq. (14). The threshold $\mathscr{T}$ for the length of the left and right segments $\mathscr{L}$ and $\mathscr{R}$ has been set to 25. Note that the threshold is a user-defined parameter, that is tuned such that all short line segments are not included in the characteristic line segments, while the long line segments are included. The fact that the threshold is higher than in the clamped plate analysis can be understood from the higher resolution in the frequency band, so that the characteristic line segments are longer. With the $\mathscr{V}_{\text{sum}}(k)$, defined in Eq. (18), it has been found that the principal diagonal is spanned by the parameter pair $[X_{\text{left}}, X_{\text{right}}]$ at the indices $(k, 2^n + 1 - k) = (2, 7)$ on the TM's DOE; this corresponds to columns 2 and 7 of Eq. (6); X_{left} is thus found at $(a_1^{(0)}, a_2^{(0)}, b_3^{(0)})$ and X_{right} at $(b_1^{(0)}, b_2^{(0)}, a_3^{(0)})$. The following selection criteria for the principal diagonal have been found:

- The maximal value of $\mathscr{V}_{\text{sum}}(k)$ is attained at $k = 2$: $\mathscr{V}_{\text{sum}}(2) = 94.9\%$.
- The second highest value of $\mathscr{V}_{\text{sum}}(k)$ is attained at $k = 1$: $\mathscr{V}_{\text{sum}}(1) = 51.2\%$, clearly less than $\mathscr{V}_{\text{sum}}(2)$.
- The opposite combination $(7, 2)$ yields a very low value of $\mathscr{V}_{\text{sum}}(7) = -334.6$.

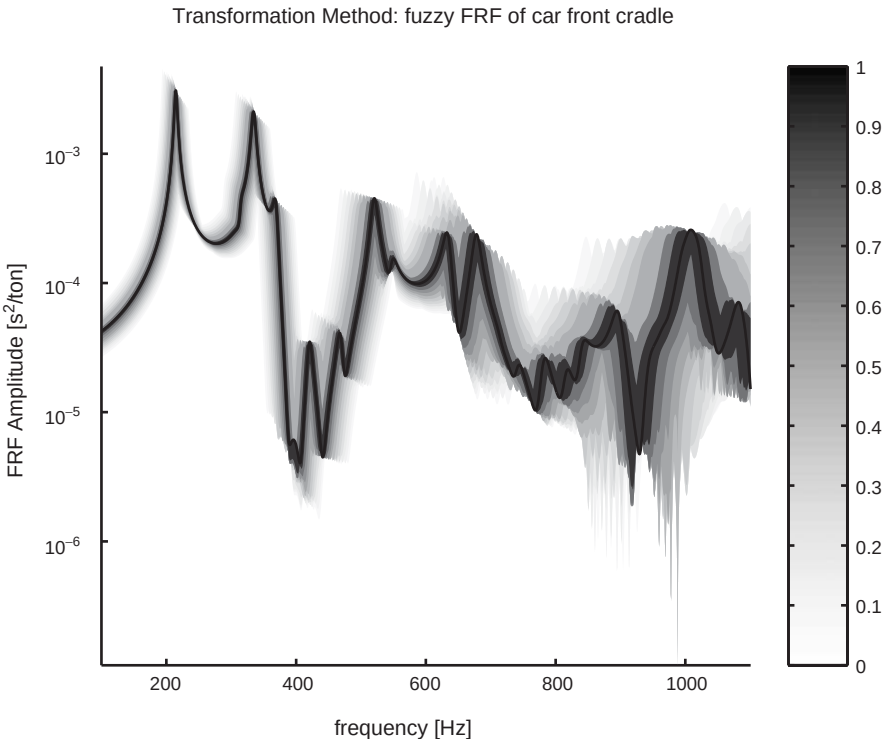

Fig. 17. Fuzzy FRF of the car front cradle in Fig. 16, obtained with the Transformation Method in the range 100–1100 Hz. A darker colour represents a higher level of membership of the fuzzy FRF output.

For higher levels of membership, only the two parameter combinations on the principal diagonal have been evaluated, i.e. $(a_1^{(j)}, a_2^{(j)}, b_3^{(j)})$ and $(b_1^{(j)}, b_2^{(j)}, a_3^{(j)})$ for $j = 2..m$, yielding $2 \cdot (m-1) = 18$ additional deterministic experiments; in total, $\mathscr{N}_{\mathrm{STM}} = 1 + 2^n + 2 \cdot (m-1) = 27$ deterministic computations are performed by the STM. For the obtained set of deterministic FRF vectors, Eq. (13) has been used to reconstruct the fuzzy FRF, which is shown in Fig. 18.

In Section 9.5, the results with the STM are given for other diagonal selections than the principal diagonal. For the purpose of ranking the 4 diagonals after the initial DOE, note that the third highest value of $\mathscr{V}_{\mathrm{sum}}(k)$ is attained at $k = 4$ ($\mathscr{V}_{\mathrm{sum}}(4) = 5.89\%$) and the fourth highest value at $k = 3$ ($\mathscr{V}_{\mathrm{sum}}(3) = -57.9\%$). The principal diagonal at combination $(2, 7)$ has the highest ranking, followed by the diagonals at combinations $(1, 8)$, $(4, 5)$ and finally $(3, 6)$.

9.4. Validation and assessment

The FRF data samples of $\mathscr{N}_{\mathrm{MC}} = 500$ Monte Carlo simulations, uniformly distributed over the input vertex (i.e. the Input range in Table 4), are used to validate the fuzzy FRF of the TM and the STM, respectively, with the criteria defined in Section 6. The results are given in Table 5. Also

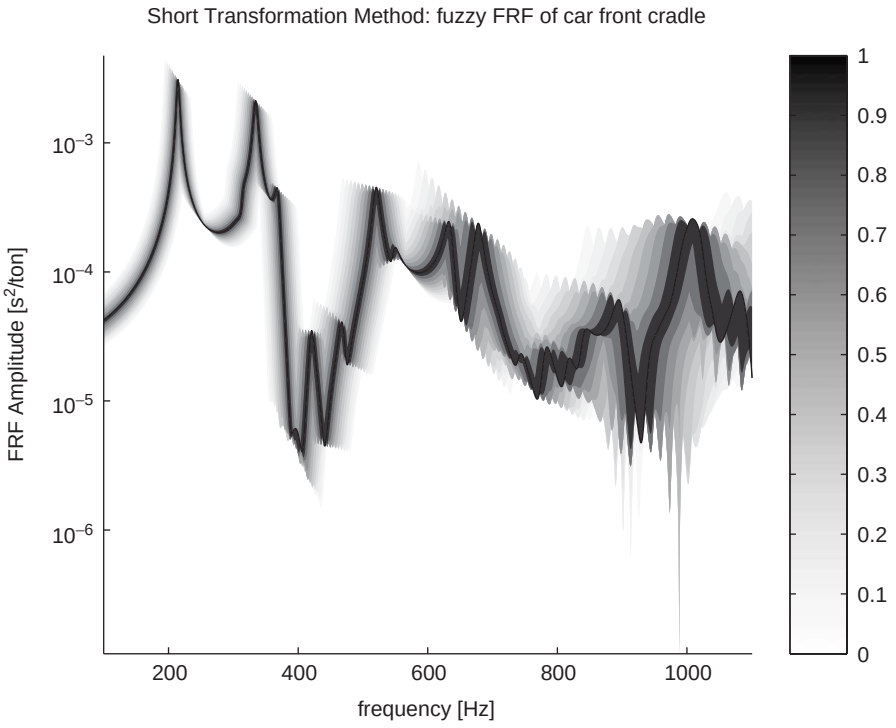

Fig. 18. Fuzzy FRF of the car front cradle in Fig. 16, obtained with the Short Transformation Method in the range 100–1100 Hz. A darker colour represents a higher level of membership of the fuzzy FRF output.

for the analysis of the car front cradle, the STM is more effective than the TM, as it reduces the number of experiments with a factor 3, again with only a slight loss of accuracy.

9.5. Justification of the proposed diagonal selection

The car front cradle is a more complex structure than the clamped plate in Section 8. The cradle has both bending modes and torsion modes that alternate with each other in the evaluated frequency range; the order of these mixed series is not known in advance, while each series may have a different dependence on the input parameters. Predicting the combination that yields the most left and right FRF would require a detailed study of the structure and its mode shapes; this is considered to be outside the scope of this paper.

In this section, the STM analysis in Sections 9.3 and 9.4 is repeated for other diagonals than the principal diagonal. The uncertain FRF predictions with the STM are then validated with the criteria introduced in Section 6. Table 6 compares the ranking according to these validation criteria with the ranking according to the $\mathscr{V}_{\mathrm{sum}}(k)$ (see Section 9.3). Again, the principal diagonal produces the best prediction of the fuzzy FRF, with the best validation against Monte Carlo data. For the other diagonals, there's a complete agreement between the rankings based on $\mathscr{V}_{\mathrm{sum}}(k)$ and the validation criteria.

Table 5
Front cradle: validation of TM and STM envelopes against Monte Carlo data

Transformation Method $\mathcal{N}_{TM} = 81$ experiments	Short Transformation Method $\mathcal{N}_{STM} = 27$ experiments
$OIP_{TM} = 98.8\%$ $\mathcal{V}^{up}_{TM}(\overline{A}_{MC}(f), \overline{A}_{TM}(f)) = 96.6\%$ $\mathcal{V}^{lo}_{TM}(\underline{A}_{MC}(f), \underline{A}_{TM}(f)) = 96.7\%$	$OIP_{STM} = 97.5\%$ $\mathcal{V}^{up}_{STM}(\overline{A}_{MC}(f), \overline{A}_{STM}(f)) = 96.5\%$ $\mathcal{V}^{lo}_{STM}(\underline{A}_{MC}(f), \underline{A}_{STM}(f)) = 95.8\%$

Table 6
Comparison of STM predictions of the car front cradle FRF, for all 4 diagonals that can be selected

Selected diagonal, at combination (...,...)	$\mathcal{V}_{sum}(k)$ (ranking)	Validation criteria (ranking)		
		OIP	VAF $\mathcal{V}^{up}$	VAF $\mathcal{V}^{lo}$
(2, 7), i.e. principal diagonal	94.9% (1)	97.5% (1)	95.8% (1)	96.5% (1)
(1, 8)	51.2% (2)	97.3% (2)	95.0% (2)	96.5% (1)
(4, 5)	5.89% (3)	96.4% (3)	93.9% (3)	96.4% (3)
(3, 6)	−57.9% (4)	95.0% (4)	91.9% (4)	96.4% (3)

The results and ranking based on the $\mathcal{V}_{sum}(k)$ criterion are compared with the results and ranking based on the OIP and VAF, i.e. the validation criteria of the fuzzy FRF against Monte Carlo data.

The agreement between the rankings is higher for the car front cradle analysis than for the clamped plate analysis (compare Table 6 with Table 3). Note that in the car front cradle analysis, there's a higher difference between the $\mathcal{V}_{sum}(k)$ values obtained at the different diagonals. The clearer distinction in the ranking of the STM results is therefore not surprising.

10. Conclusions

In the present paper, the Transformation Method (TM) of M. Hanss has been applied to predict the effect of input uncertainty on the FRF of structures under dynamic loading. The method designs a set of deterministic experiments to numerically approximate the fuzzy FRF vector. This allows to solve the bulk part of the structural dynamics analysis with existing Finite Element routines. The TM results have been validated against FRF data samples from a sufficiently high number of Monte Carlo simulations in the same input parameter range. For the considered structures, it has been shown that the TM yields envelopes that are almost, but not fully conservative: the non-monotonicity of the FRF amplitudes and the TM's sampling procedure have the effect that some (anti-)resonance peaks are simply missed, resulting in saw-like shapes of the global FRF envelopes. As these shapes can easily be recognized, this undesired effect does not limit the TM's applicability to assess the effect of input uncertainty, provided that a

sufficiently high number of interval levels (typically 5 to 10) is set for the TM's Design of Experiments. The computational burden of the TM may become too high when a structure has a large number of uncertain input parameters or when a large computation time is required for a single deterministic computation. The short transformation method (STM) is presented in this paper as an attractive alternative to the original TM for frequency domain applications. Significant reductions in computation time have been achieved.

Starting from the assumption that input uncertainty results in monotonic eigenfrequency shifts for the dynamic structure under consideration, the STM has been designed as a two-step procedure. First, the FRF vectors are computed for the input vertex combinations and the core combination (i.e. the original TM is applied with $m = 1$ levels of membership), yielding an initial set of FRF vectors. Starting from the global FRF envelope of this set, a heuristic procedure is used to find the parameter combination pair on the input vertex with the largest effect on the global FRF envelope. More specifically, the global FRF envelope is reduced to two sets of characteristic line segments on the left- and right-hand side of the global envelope. When a parameter combination on the input vertex has the largest shape conformity with one side of the global envelope, it can be expected that the opposite parameter combination has the largest contribution to the other side of the global envelope. This allows to select the principal diagonal in the parameter hyperspace. For higher levels of membership (typically 5–10 levels), the STM selects only the 2 parameter combinations along this principal diagonal for further analysis. As the TM computes a Full Factorial DOE of 2^n experiments for the higher levels of membership, the STM results in a significant reduction of the computation time. Moreover, the reduction percentage increases exponentially with the number of input parameters.

For the considered structures, it has been shown that the STM predicts the fuzzy FRF from a much smaller set of computations, with only a small reduction in accuracy of the validation criteria against Monte Carlo FRF data. Apparently, the assumption of eigenfrequency monotonicity is valid for the considered structures. Furthermore, the STM results have been repeated for other diagonal selections than the principal diagonal. For both structures, selecting another diagonal than the proposed principal diagonal yielded less accurate predictions of the uncertain FRF—a justification of the selection procedure of the principal diagonal. Finally, note that the STM evaluates a subset of the TM's DOE. One might therefore consider to apply the STM as a first phase of any uncertainty assessment with the TM; when a higher accuracy is desired, the TM analysis can be completed by evaluating the remaining parameter combinations of the TM's DOE.

Acknowledgements

This work was made possible under the IST Marie Curie Industry Host Fellowship "VIPROM", from which the first author received a grant. It has been the aim of this research project to develop Finite Element methods for the "medium frequency range" (e.g. 200–600 Hz for cars). The effects of parameter variability and uncertainty become increasingly important in this range, hence the interest in the topics addressed in this paper. The European Commission is greatly acknowledged for their support.

References

[1] W.L. Oberkampf, K.V. Diegert, K.F. Alvin, B.M. Rutherford, Variability, uncertainty and error in computational simulation, *AIAA/ASME Joint Thermophysics and Heat Transfer Conference*, *ASME-HTD*, vol. 357(2), 1998, pp. 259–272.

[2] T.A. Zang, M.J. Hemsch, M.W. Hilburger, S.P. Kenny, J.M. Luckring, P. Maghami, S.L. Padula, W.J. Stroud, Needs and opportunities for uncertainty-based multidisciplinary design methods for aerospace vehicles, Technical Report NASA/TM-2002-211462, NASA, Langley, Virginia, USA, July 2002.

[3] D. Moens, A Non-probabilistic Finite Element Approach for Structural Dynamic Analysis with Uncertain Parameters, PhD Thesis, KU Leuven, Leuven, Belgium, October 2002.

[4] M. Hanss, K. Willner, On using fuzzy arithmetic to solve problems with uncertain model parameters, in: *Proceedings of the Euromech 405 Colloquium*, Valenciennes, France, 1999, pp. 85–92.

[5] S.S. Rao, J.P. Sawyer, Fuzzy finite element approach for the analysis of imprecisely defined systems, *AIAA Journal* 33 (12) (1995) 2364–2370.

[6] B. Lallemand, A. Cherki, T. Tison, P. Level, Fuzzy modal finite element analysis of structures with imprecise material properties, *Journal of Sound and Vibration* 220 (2) (1999) 353–364.

[7] S.S. Rao, L. Berke, Analysis of uncertain structural systems using interval analysis, *AIAA Journal* 34 (4) (1997) 727–735.

[8] D. Moens, D. Vandepitte, Envelope frequency response function calculation of uncertain structures, in: *Proceedings of ISMA 25*, 2000, pp. 395–402.

[9] A.I. Khuri, J.A. Cornell, *Response Surfaces, Design and Analysis*, second ed., Marcel Dekker, New York, USA, 1996.

[10] W.M. Dong, H.C. Shah, Vertex method for computing functions of fuzzy variables, *Fuzzy Sets and Systems* 24 (1) (1987) 65–78.

[11] M. Hanss, The Transformation Method for the simulation and analysis of systems with uncertain parameters, *Fuzzy Sets and Systems* 130 (3) (2002) 277–289.

[12] W. Heylen, S. Lammens, P. Sas, *Modal Analysis Theory and Testing*, second ed., Katholieke Universiteit Leuven, Department of Mechanical Engineering, 1997.

[13] H. Koivo, Fuzzy Logic Systems, *Lecture Notes AS-74.115 on Neuro-Fuzzy Computing in Automation*, Helsinki University of Technology, January 2001, http://www.control.hut.fi/Kurssit/as-74.115/Material/index.html.

[14] S. Donders, J. Van de Peer, L. Hermans, Application of the transformation method for the analysis of finite element models with uncertain model parameters in the automotive industry, in: *Proceedings of NAFEMS*, Wiesbaden, Germany, May 7–8, 2003.

[15] J.E. Dennis Jr., R.B. Schnabel, *Numerical Methods for Unconstrained Optimization and Nonlinear Equations*, Prentice-Hall, Englewood Cliffs, England, 1983.

[16] V. Verdult, *Nonlinear System Identification*: *A State-Space Approach*, PhD Thesis, University of Twente, 2002.

[17] The MathWorks Inc., MATLAB Version 6.5, June 2002.

[18] Noesis Solutions, OPTIMUS Rev 4.0, March 2003.

[19] MSC, MSC/Nastran 2001, February 2001.

[20] LMS International, LMS Virtual.Lab Rev 3, October 2003.